Microsyst Technol
DOI 10.1007/s00542-013-2054-y

TECHNICAL PAPER

Flexible hot-film anemometer arrays on curved structures for active flow control on airplane wings

M. Schwerter · T. Beutel · M. Leester-Schädel · S. Büttgenbach · A. Dietzel

Received: 9 August 2013 / Accepted: 18 December 2013

Abstract A set of flexible MEMS sensor arrays for flow measurements in boundary layers is presented. The sensor principle of these anemometers is based on convective heat transfer from a hot-film into the fluid. Each sensor consists of a nickel sensing element between copper supply tracks. The functional layers are attached either on a ready-made polyimide foil or on a spin-on polyimide layer. These variants are designed to meet the requirements of measurements in different environments. Spin-on technology enables the use of very thin polyimide layers, ideally suited for measurements in transient flows. It is a unique characteristic of the presented arrays that their total thickness can be scaled from 7 to 52 μm. This is essential, because the sensor thickness has to be adapted to the varying thickness of the boundary layers in different aerodynamic tests. With these sensors we meet the special requirements of a wide range of fluid mechanic experiments but in particular those of future active flow control on airplane wings. For less critical flow conditions with much thicker boundary layers, thicker sensors might be sufficient and cheaper, so that sensors fabricated on ready-made foils are perfect for these applications. Since the presented sensors are flexible, they can be attached on curved aerodynamic structures without any geometric mismatches. The entire development, starting from theoretical investigations, is described. Further, the micro-fabrication is discussed, including photolithography, sputtering and wet-etching. In particular the wet-etching of the sensing element is found to be critical for the functional characteristics.

M. Schwerter (✉) · T. Beutel · M. Leester-Schädel · S. Büttgenbach · A. Dietzel
Institute of Microtechnology, Technische Universität Braunschweig, Alte Salzdahlumer Straße 203, 38124 Brunswick, Germany
e-mail: m.schwerter@tu-bs.de
URL: http://www.imt.tu-bs.de

1 Introduction

During the last years, many micro-electro-mechanical sensor devices have been developed for measurements in fluids. They are mostly based on silicon or glass substrates measuring the wall pressure or other relevant information about the flow. Since they are fabricated on rigid substrates, only planar surfaces were achieved. In contrast, most relevant aerodynamic structures are slightly curved. Therefore, several attempts have been made to match with the conditions in different experiments on curved surfaces (Kälvesten 1996). A first approach was to minimize the size of the rigid sensors in order to reduce the geometric mismatch between the sensors and the aerodynamic model. An example is given in (Berns et al. 2008), where silicon based pressure sensors, smaller than 2×2 mm^2 each, were closely spaced on a round shape. However, these are manually bonded onto a printed circuit board (PCB), while the gaps are filled with glue. This procedure requires extensive assembly work. In a second approach, researchers are using 3D-elements which are deflected out of the wafers' plane using shape memory alloys or shrinking processes in order to create a 3D-hot-wire sensor for flow velocity measurements (Ebefors 2000). Recent developments led to small hotplates (Mailly et al. 2001), having a very low heat transfer into the substrate. However, all reported sensors still were made on rigid substrates.

In a new field of aerodynamic research, laminar wings are becoming more and more interesting. Here the drag is reduced by keeping the flow laminar, which requires a well-defined profile. Geometric discrepancies between the desired smooth contour and the real shape have to be avoided. Additionally, in the field of active flow control (AFC) new sensors are required. In AFC the flow is

Published online: 14 January 2014

influenced by actuators. In order to build up a closed loop control, fast sensors have to be installed. They must be mounted flush to the wall, not influencing the flow themselves (Gad-El-Hak 2001; Morrison et al. 2006).

All these parameters led to novel sensor concepts enabling fast, accurate, reliable and non-intrusive measurements. The advances in flexible substrate technologies seem to be an enabler for this kind of sensors. In the past, many flexible pressure sensors have been presented to be used as a tactile skin in robotic applications, for example sensors based on polydimethylsiloxane (PDMS) (Riedl et al. 2009). These sensors also became popular in aerodynamic measurements, but their use is limited due to the relatively low sensitivity.

For aerodynamic measurements, a different sensor concept has been presented, namely a wall shear stress sensor (Buder et al. 2006). The working principle is based on heat transfer from a heated film into the fluid, similar to a hot-wire anemometer (King 1914). It is fabricated on polyimide because of its good stability over a wide temperature range. Commercial devices are available (Tao of Systems Inc. and Dantec Dynamics A/S) with sensor elements made of nickel deposited on a polyimide foil with a thickness of 50 μm. However, these commercially available arrays are not optimized regarding the heat losses into the substrate or regarding their dynamic behavior. Therefore, a flexible sensor has been presented, on which the thermal transport mechanisms have been simulated and later been improved by dry-etching the substrate underneath the sensing element (Buder et al. 2006). The same group presented a sensor having the contact pads on bottom side, giving more options for the possibilities of electrical connections. The drawback of the sensor is the mechanical instability of the exposed hot-wire.

Nowadays, for wind tunnel experiments researchers still need to include cavities in their aerodynamic model constructions, in which the commercially available 50 μm thick polyimide patches can be placed. The problem with this procedure is that every alignment error leads to a gap or a step causing incorrect measurements. To avoid these shortcomings, the total height of the sensor needs to be reduced.

The flexible sensor arrays presented here rely on the same principle as described in Buder et al. (2006), but substantial improvements have already been realized. Their total thickness can be adapted in a wide range to meet the requirements of different experiments. Due to the array layout, the spatial resolution is much higher than those of a series of single sensors. The possible reductions in critical dimensions should also positively influence sensitivity and dynamical behavior.

2 Theory

The theory describing the sensing effect of hot-film anemometers is widely known. Early measurements have been performed by King (1914). The principle is based on heat transfer from a heated wire or film into the fluid to be measured. In a single conductor with an electrical resistance R the consumed electrical power P is inserting heat. This heat flow depends on R and the current I (Eckelmann 1997):

$$P = R \cdot I^2 \tag{1}$$

The inserted heat will be dissipated into the ambient in three modes of heat transfer. The first mode is heat conduction. As described in Eq. (2) the conductive heat flow $Q_{conduction}$ is conducted through an object with the cross-section A in the presence of a temperature gradient dT/dx. For example one part of the heat from the resistor may be conducted through the connecting wires out of the system boundaries. The ability of conducting heat for a certain material is described by the thermal conductivity k.

$$Q_{conduction} = -kA\frac{dT}{dx} \tag{2}$$

The second mode is heat convection. The convective heat flow $Q_{convection}$ depends on the heat transfer coefficient h, the surface area A and $T–T_{fluid}$, the temperature difference between the resistor and the surrounding fluid, as shown in Eq. (3). It may be noticed that h also depends on $T-T_{fluid}$.

$$Q_{convection} = hA(T-T_{fluid}) \tag{3}$$

The third mode is radiation. Depending on the emissivity ε, the surface A and the temperature T of an object part of the power can be dissipated this way (Lienhard IV and Lienhard V 2005) as described in Eq. (4). σ represents the Stefan-Boltzmann constant. In the context of heated sensors it has to be underlined that the radiation $Q_{radiation}$ increases with the fourth power of the temperature.

$$Q_{radiation} = \varepsilon\sigma AT^4 \tag{4}$$

With the small surface of the hot-film, a material with low emissivity ε and a temperature below 600 K the contribution of radiation is comparatively small and the heat flow due to radiation can be neglected.

The dissipated power P_{diss} is equal to the sum of the three dissipating heat flows described by Eqs. (2)–(4). Having time variable velocities the influence of the capability to store thermal energy has to be considered, as well. The associated temporary heat flow $Q_{capacity}$ depends on the wire's mass m, the heat capacity c and the time variable temperature rise $\frac{d(T-T_{fluid})}{dt}$ as

$$Q_{capacity} = mc\frac{d(T - T_{fluid})}{dt} \tag{5}$$

Applying an electrical power P to the sensor the temperature increases continuously until the sum of all heat flows again reaches zero which means that a steady state is achieved as expressed in Eq. (6). For the function of an anemometer sensor the heat convection shall be the dominating heat dissipation mode. It is essential for the sensor function that the heat transfer coefficient h is not constant; it depends on the flow velocity and the condition of the flow (laminar, turbulent). This relation is used as the anemometric sensing effect. For typical hot-film materials the temperature coefficient is positive, so the resistance increases with the temperature.

$$P = R(T) \cdot I^2 = hA\left(T - T_{fluid}\right) + kA\frac{dT}{dx} + mc\frac{d(T - T_{fluid})}{dt} \tag{6}$$

As it can be seen in Eq. (6), both a change of h and of T_{fluid} affect the resistance and the current in operation. By the design the sensor's surface A can be adapted to reduce or increase the surface for heat transfer. The undesired conduction through the substrate can be reduced by selecting a material with a lower k or with increasing the substrate's thickness x in case the anemometer will be attached to a body with higher k. The heat capacity c and the mass m of the sensing element may be adjusted to improve the high frequency behavior.

A more empiric equation describing hot-wire behavior can be found in (Eckelmann 1997). Here, the coefficients B, C and n have to be obtained from experiments to link the heat loss with the fluid density ρ, the fluid velocity U and the temperature difference $T-T_{fluid}$:

$$R(T) \cdot I^2 = \left(B + C(\rho U)^{1/n}\right) \cdot (T - T_{fluid}) \tag{7}$$

Depending whether I or T is set to constant in Eqs. (6) or (7) two different operation modes can be distinguished:

2.1 Constant current anemometry

The hot-film is part of a Wheatstone bridge (Fig. 1a). A (nearly) constant current through the bridge is given by R_V. When changing the heat transfer coefficient h the temperature T adapts with the new ability to dissipate heat. The resistance R, which depends on T, changes itself, too, but in a relatively small range. An amplifier compares the voltage drop over the hot-film with the voltage drop over a selectable resistor in the other part of the Wheatstone bridge and amplifies it.

The constant current anemometry can be used to measure variations in velocity or temperature. On contrast, it is not suitable for wide fluid velocity ranges due to a decrease of sensitivity when using the circuit for much higher velocities than the calibrated one. When measuring much lower velocities the sensor may overheat and destroy itself.

2.2 Constant temperature anemometry

In this mode the hot-film sensor is part of a Wheatstone bridge, too. As in the constant current anemometry an amplifier compares the voltages in the bridge and amplifies the difference. Using a feedback a closed loop control is realized to hold the temperature difference $T-T_{fluid}$ constant. Changes in h affect the current I, which can be measured directly at the amplifiers output (Fig. 1b).

The constant temperature anemometry has a non-linear behavior too. But in contrast to the constant current anemometry this non-linearity is lower. Due to the closed loop the sensor is protected against overheating (Eckelmann 1997; Burkhardt 2004).

Furthermore, several sensor parameters may be adjusted in the design or operation, for example the area of the

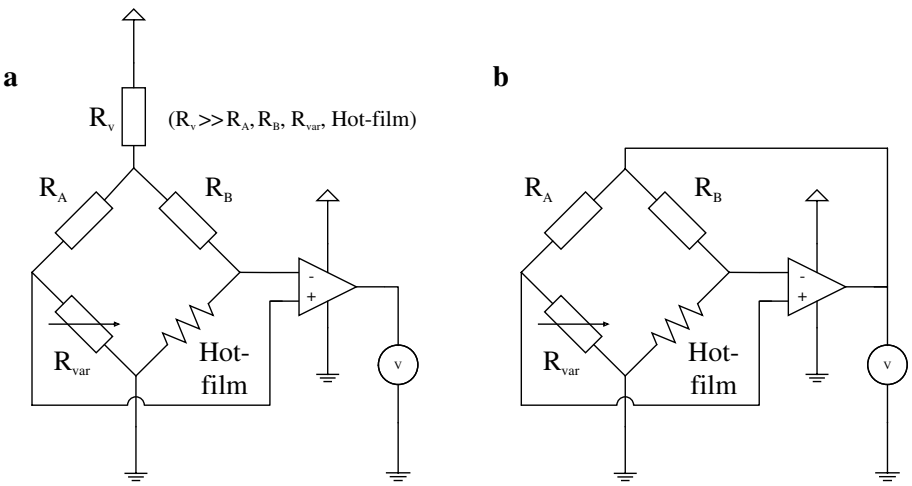

Fig. 1 Electrical circuits for constant current anemometry (**a**) and constant temperature anemometry (**b**)

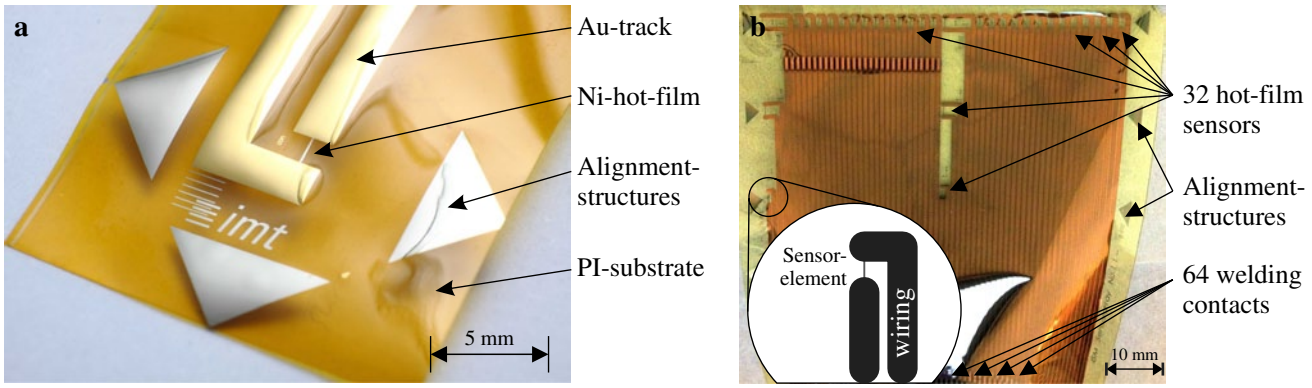

Fig. 2 Photos of a single element sensor on ready-made foil (**a**) and a sensor array processed on spin-on polyimide (**b**)

heating surface or the temperature of the hot-film. The ratio $Q_{convection}/P_{diss}$ may be adjusted by changing the amount of $Q_{conduction}$, which can be done, for example, by using sensors substrates or wiring materials with different thermal conductivities or thicknesses. Reducing $Q_{conduction}$ will increase the sensitivity and dynamic range of the sensor because of heat stored in the substrate (the gradient $\frac{dT}{dx}$ is time dependent and can assume different polarities).

3 Fabrication

In order to vary the total thickness of the array, an appropriate polyimide foil substrate can be chosen. Ready-made foils are available in thicknesses of 25 and 50 µm (Kapton HN, DuPont), enabling very robust sensors as shown in Fig. 2a. This process is very cost effective. The sensing element and the tracks do not exceed 2 µm thickness. However, this relatively thick sensor cannot be used on laminar wings, because the critical boundary layer might be affected as flush fitting cannot be obtained, which is not acceptable for AFC applications.

To eliminate this drawback, spin-on polyimides were investigated. With the polyimide used here, layer thicknesses of 5 µm are achievable by a spin-on process. Fabricating thicker layers in one step results in a higher stress making the sensors curling after the release from the substrate—however, by repeating the spin-on step after curing the polyimide layer in a vacuum oven, thicknesses of up to 25 µm can be obtained. Figure 2b shows an array on 20 µm thick spin-on polyimide. Using the spin-on approach, the minimum sensor thickness was reduced down to 7 µm. To the knowledge of the authors, this has never been demonstrated before. Of course, this reduces the mechanical stability but the polyimides' tensile strength is relatively high (~350 MPa).

The proposed sensor arrays (B) are fabricated in a batch process developed specifically for this design using state-of-the-art microsystem technologies. Figure 3 illustrates the most significant steps of sensor fabrication on ready-made foil (A) and on spin-on polyimide (B). Polyimide is in both cases the material of choice because of its thermal stability, its resistance to chemicals and its mechanical robustness. Additionally the heat conduction of polyimide is only around one thousandth of silicon and of the most metals (DuPont 2011; Haynes 2010).

In version A the glass substrate has to be cleaned and afterwards the polyimide foil is bonded onto the wafer (A1). The hot-film material (Ni) layer is then magnetron sputtered (A2) directly onto the substrate. The thickness of the sputtered metal layer determines the resulting height of the hot film *h*. Afterwards, a first photolithography step is carried out and the metal is wet-etched. The lateral dimensions of the sensing elements are thereby defined. In step 3, the seed layer for the electroplating process is sputtered onto the substrate material. The area which is not part of

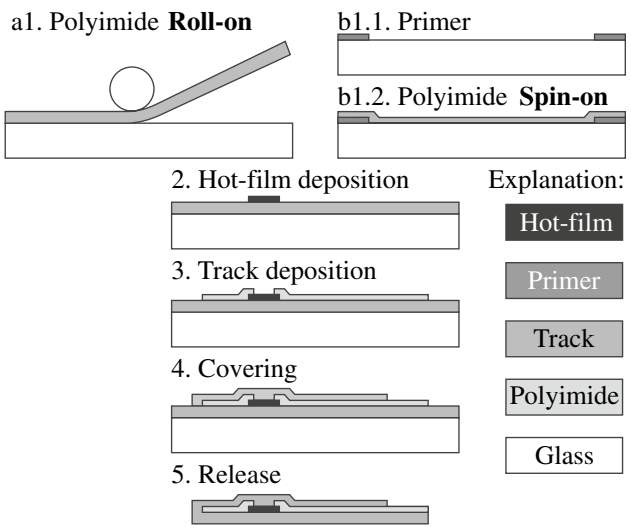

Fig. 3 Significant process steps starting with ready-made polyimide foil (**a**) or spin-on polyimides (**b**)

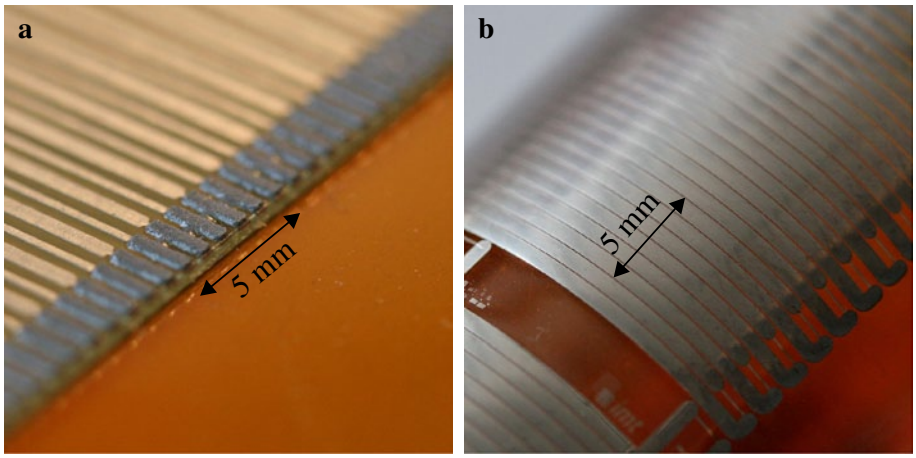

Fig. 4 Soldering paste on board for reflow soldering (**a**), hot-film on curved surface (**b**)

the supply conductors (tracks) is covered with photoresist; the tracks are electroplated with copper until a layer thickness of 2 µm is reached. After that the tracks may to be protected against oxidation with a thin layer of electroplated nickel or plated tin. Then the remaining seed copper has to be wet-etched.

The adhesion of the nickel as well as the copper can be enhanced by sputtering a thin layer of chrome directly before the nickel or copper sputtering. Certainly this layer also needs to be removed during structuring the hot-films or tracks.

Finally, a foil area including the sensors and tracks can be cut out and peeled off from the rigid substrate. Step 4 is optional and only applied if the sensor array needs a protective cover, e.g. for measurements in water. This increases the robustness, but influences the dynamic sensor behavior. Different materials for covering may be suitable, like different silicon oxides or parylene (Burkhardt 2004) or another layer of polyimide.

In version B a spin-on polyimide (PI-2611, HD Microsystems, LLC) is used to fabricate a 5 µm thick layer. To increase the stability a primer is applied near the edge of the wafer. To produce the polyimide-layer it is spun-on first. Then it has to be soft-baked on a hotplate. After that it is cured at a temperature of 350 °C in a vacuum oven. For detailed processing see (HD MicroSystems 2009). By applying more than one layer of polyimide, different layer thicknesses are achievable. In this case the next layer may be applied just after the soft-bake of the prior layer. Otherwise the already cured polyimide has to be dry-etched in an O_2-plasma to roughen the surface for better adhesion.

For a high quality of the sensors, especially for homogeneous resistance values in an array of sensors, it is essential to use accurate photolithography and to wet-etch the nickel-layer precisely. Most of the defects observed are produced during these critical process steps. The very first version of the array on spin-on polyimide was realized with at that time available TiW material for the sensing elements (Fig. 2b). In later versions, arrays with Ni elements were fabricated.

Covering layers made of liquid polyimide can be partly opened by etching in O_2-plasma. In this way the sensing elements may be uncovered using a photoresist mask with appropriate openings.

For proper and long-lasting measurements a reliable connection between the sensor and the measurement circuit is essential. The first connections were made by hand soldering thin copper wires to connect the foil pads with the board pads. The procedure is very time-consuming, but the connection is fragile and is not suited for tests on wind tunnel models.

Having a foil with tracks the connection may also be realized with zero insertion force (ZIF) connectors. These connectors can be soldered on the circuit board and easily connected. Anyway, disadvantages of the connectors are the non-fitting number of pins (several smaller connectors may be used), the volume of the connector and the fixed pitch limiting the design freedom.

To enable a very flat connection a reflow soldering process may be used. Here the sensor is directly soldered on the board. Therefore, a soldering paste is applied through a stencil on the board (Fig. 4a) and, after that, the sensor is attached. Using a reflow oven or a hot plate the solder paste is melted. After cooling down it connects sensor and board properly.

The hot-films were mounted on flat surfaces as well as on curved structures. Figure 4b shows a sensor mounted on a tube with a radius of 15 mm. Subsequent tests confirmed the operational reliability.

4 Tests and results

To avoid interferences with a more complex processing on polyimide first tests were performed with sensors on glass substrates. The cold resistance as well as the temperature

coefficient were evaluated for sensors made with different sensing element materials.

4.1 Cold resistance and resistivity

The cold resistance R_0 can easily be measured by using a multimeter (current almost zero) without inserting the hot-film in a climate chamber or adding other electronic components. The cold resistance is defined by geometric properties (length l and cross section A) and the resistivity ρ of the hot-film material:

$$R_0 = \rho \cdot \frac{l}{A} \tag{8}$$

For approximate calculation the cross section A can be defined as the film's width b multiplied by its height h, which is the layer thickness of the sputtered hot-film material. Having in mind that the hot-film is etched out of this material, the behavior of the etching acid has to be considered to get a more precise value for the cross section A and subsequently for the resistivity.

As shown in Fig. 5 the wet etching of the resistor material leads to an undercut in the shape of a quadrant. With the given hot-film dimensions a mismatch of up to 14 % may occur when assuming a rectangular cross-section. By subtracting the undercut area from the origin cross section, a more suitable calculation is given by:

$$R_0 = \rho \cdot \frac{l}{bh - \frac{1}{2}\pi h^2} \tag{9}$$

By measuring the resistance of different hot-films the resistivity ρ of the deposited material can be calculated with Eq. (9). As it can be seen in Fig. 5b the actual cross shape is not completely regular due to stochastic phenomena in the etching and due to the edge blurring of the covering photoresist. But calculated values were sufficiently accurate. Thereby determined resistivity of some common hot-film metals compared to bulk material literature values are shown in Table 1. Deviations are caused by the deposition process, which was—in this case—magnetron sputtering (De Vries 1988). These influences are much higher than the influences due to mismatches of the underlying dimension.

Table 1 Measured resistivities of different metals at 20 °C compared to literature values for bulk materials

Material (a–z)	Resistivity ρ (Ωm) from experiment	Resistivity ρ (Ωm) from (Haynes 2010; Frühauf 2005a, b; Shackelford and Alexander 2001)
Aluminum (Al)	$7.45 \cdot 10^{-8}$	$2.65–2.9 \cdot 10^{-8}$
Gold (Au)	$6.46 \cdot 10^{-8}$	$2.1–2.4 \cdot 10^{-8}$
Nickel (Ni)	$29.70 \cdot 10^{-8}$	$6.5–9.5 \cdot 10^{-8}$
Titanium (Ti)	$197.00 \cdot 10^{-8}$	$42.0–47.0 \cdot 10^{-8}$

Given these resistivity values of sputtered material the still adjustable parameters are the length of the sensing element, the height and the width where the under etching phenomena have to be considered.

4.2 Temperature coefficient of resistance

The thermal coefficient of resistance α defines the resistance change with increasing temperature. To achieve a high sensitivity of the sensor the value of α of the selected hot-film material has to be as high as possible. Values of α for different bulk materials are shown in Table 2, right column. α is related to a resistance R_{ref} at the reference temperature T_{ref}:

$$\alpha = \frac{1}{T - T_{ref}} \cdot \left(\frac{R}{R_{ref}} - 1 \right) \tag{10}$$

The thermal coefficient of the sputtered hot-film material was experimentally determined by heating the sensors in a climate chamber. To avoid a forced air movement above the sensor elements a cover was placed over the

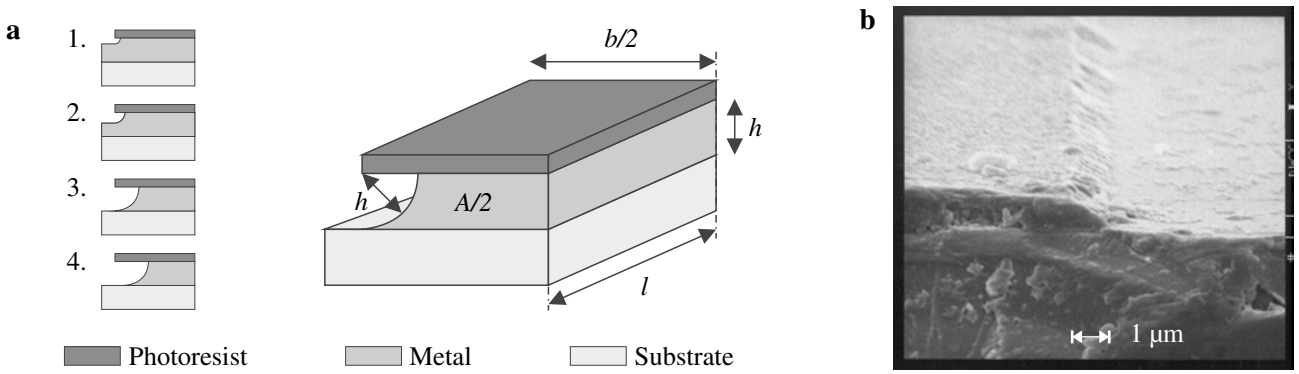

Fig. 5 Isotropic etching of the metal layer leads to an undercutting of the masking layer (photo resist)

Table 2 Measured α of different metals at $T_{ref} = 293$ K compared to bulk material literature values

Material (a–z)	α (1/K) from experiment	α (1/K) from (Rohlfing and Schmidt 1993)
Aluminum (Al)	0.0031	0.0039
Gold (Au)	0.0028	0.0039
Nickel (Ni)	0.0049	0.0067

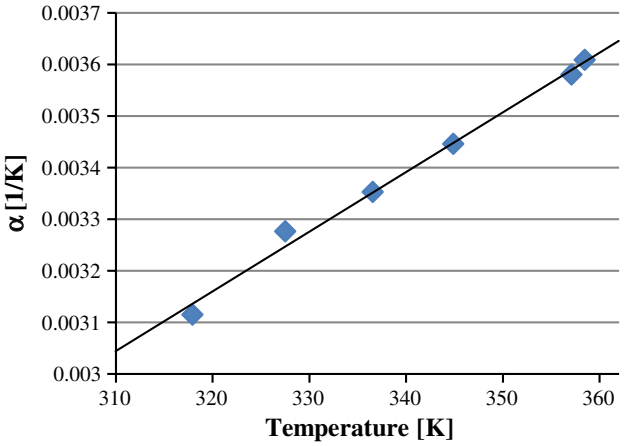

Fig. 6 Temperature coefficient of resistance α vs. hot-film temperature T

array. The sensor's temperature T was measured next to the sensor elements. The temperature coefficients found by linear regression in a very small temperature range around the reference temperature $T_{ref} = 293$ K for different materials are shown in Table 2, center column.

For the operation of a sensor a wider temperature range has to be considered and a linear function $R(T)$ cannot be assumed anymore. Therefore additional measurements at up to 360 K were performed from which the local gradients $\alpha(T)$ were obtained (Fig. 6). The measurements showed a linear rise of α with increasing temperature. These measurements were performed with Ni-sensors on polyimide substrates. The α value at 293 K is lower than the one obtained on glass indicating a less perfect thin film microstructure. However, in the constant-temperature mode and in cases with only small sensor temperature changes, a constant α can be assumed and taken from Fig. 6.

The temperature coefficient of resistance for each sensing element of the sensor array can also be automatically evaluated using a closed loop oven. Several temperature-resistance-pairs are measured by the following procedure. First the oven is set to the desired temperature. After maintaining a stable temperature the resistance for each sensing element is measured. The values are used in the calculation of the temperature-resistance-function for each sensor array to be calibrated. Finally, after finishing the measurement, the temperature coefficient of resistance can be calculated for the desired operating point using this function.

4.3 Water reliability

For measurements in water tunnel experiments the robustness against water is required. The currents in the hot-film sensor are, compared to other MEMS sensors, relatively high, so electrochemical effects in contact with water cannot be excluded.

In order to quantify the behavior in water two sensor arrays were inserted in a water chamber over 2 months and energized for 1 h each day. This schedule represents a measurement campaign in water tunnels.

Two sensor arrays were covered using two different materials. The first covering was realized using electroless plated tin which deposits on the conducting elements only. On a second sensor array an almost homogeneous layer of 5 µm polyimide was spun-on and cured. The polyimide coverage over the sensing elements was locally etched away for better sensitivity.

For comparison not all sensor elements of each array were energized. The results of visual inspection are shown in Fig. 7. The tin-covered sensor (A) was damaged due to electro migration effects. This is proven by the observation that the tracks connected to the negative terminal of the power supply lost their tin. Some of the tracks were

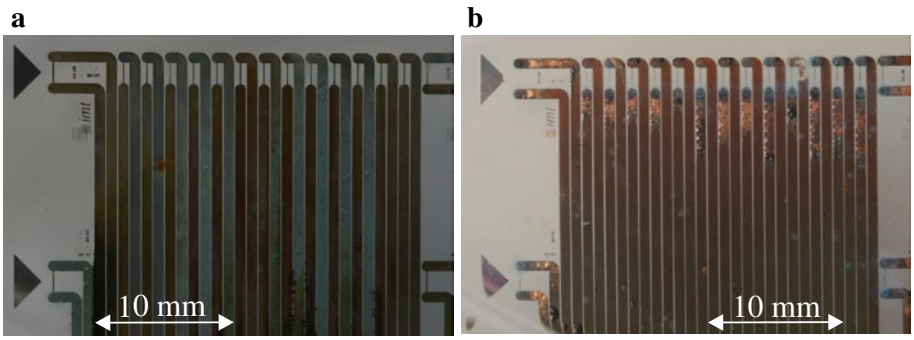

Fig. 7 Sensors covered with tin (**a**) and polyimide (**b**) after 2 months operation in water

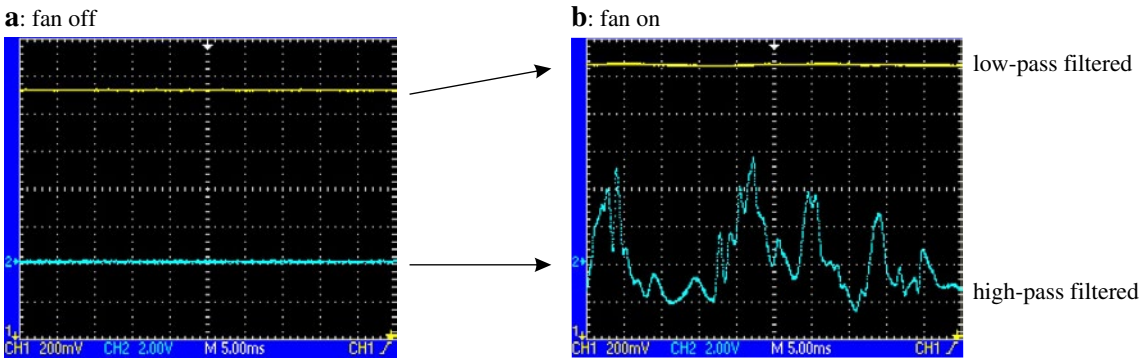

Fig. 8 Hot-film in idle operation (**a**) and blown with a fan (**b**)

connected to each other, so they are short circuited. In addition, unconnected tracks show corrosion.

After 2 months 7 of 17 tinned sensors are totally damaged, most of the other ones showed high changes in their resistance.

In Fig. 7b the polyimide-covered sensor is shown. The covering is damaged at the negative supply connections to the sensing elements. In a detailed analysis it was found out that also a small part of the copper track near the sensing element was uncovered when polyimide was locally removed during fabrication, so the copper could corrode at the negative terminal. Additionally, at some single points the polyimide was macerated. Here, water seems to be diffused through the covering. Anyway, only 2 of 20 sensors are totally broken after two months. 12 of the 18 still usable sensors changed their resistance by less than ten percent.

4.4 Dynamic tests

First functional tests were performed using an electronic circuit to operate in constant temperature mode. The output signal was high- and low-pass filtered, so both the average wind speed as well as fast, local changes in the flow field can be registered.

In Fig. 8 the low-pass filtered signal is represented by the upper graph. When blowing with a fan (B) more current is needed to keep the operating temperature, so the average current rises. The low-pass filtered signal is influenced by the heat conduction through the substrate. This leads to a damped sensor behavior observed for lower frequencies. Additionally nearby sensing elements are influenced by cross-heating.

Having a very thin polyimide substrate the material the sensor array is attached to strongly influences the sensor signal and thus the sensitivity. A wooden or plastic wind tunnel model conducts the heat less than a metal model, so the sensitivity of the sensor array used on a metal model will decrease.

The high-pass filtered signal is represented by the lower graph. Fast flow gradients will lead to temperature gradients in the vicinity of the sensor and the sensor will not reach a steady-state. Turbulent behavior can be detected but only relative changes can be obtained.

It is important to mention that the high-pass filtered signal contains additional electromagnetic disturbance as well as oscillating phenomena of the electronic circuit. The oscillation can be originated in the closed loop control and in capacities and inductances of the electronic components as also reported by Davis (1970).

An approach to clear coupled electromagnetic disturbance is to insert a cable with the length of the sensor's cable between R_{var} and the Wheatstone bridge (see Fig. 1). When mounting this potentiometer cable near the sensor's cable the electromagnetic perturbations couple in both cables the same way. This affects both parts of the Wheatstone bridge and is hence balanced.

5 Conclusion and outlook

The fabrication and processing of the sensor arrays placed on ready-made foils with good reproducibility could be demonstrated. The processing of the foil temporarily attached to a glass wafer was compatible with all relevant processes that are normally used for rigid substrate processing. Also the fabrication of sensors on ultra-thin (5 µm) polyimide layers has successfully been demonstrated utilizing nearly the full 4″ wafer area, requiring a very precise processing and fabrication.

The sensitivity of the sensing element is increased, if made of nickel, due to the 60 % higher temperature coefficient compared to aluminum or gold even though the thermal coefficients of resistance for our thin films (in particular on flexible polyimide) were slightly lower than reported for bulk materials from other groups.

The sensors can be used in water tunnel experiments for up to 2 months. The polyimide cover sufficiently protects the sensor against water. However, we found that two further improvements still need to be implemented. Firstly, the

etching area opening the cover over the sensing element has to be smaller than the sensing element itself to ensure that the copper track remains totally covered. Secondly, an additional very thin continuous layer of silicon nitride may be used as a more effective diffusion barrier to avoid penetration of water into the polyimide.

The high frequency behavior of the sensor could not be totally investigated by now. However, first results in turbulences as well as measurement results of the high frequency calibration device are promising. To evaluate the high frequency behavior more systematically and to calibrate the hot-film sensor a device using a rotating disk with flutes (as described in Kim and Lee 2006) shall in the future be used. In this device the sensor is attached on a fixed disk without flutes; the disk with flutes is rotating above the sensor in a certain distance.

In conclusion, the sensor arrays presented here enable new ways to measure in very thin flow boundary layers without disturbing them. The thinnest possible sensors are three times thinner than all other known sensors of this type. In combination with the versions on ready-made foil, these flexible sensors do fit for many more applications, for example for measurements in tubes with small diameters. By now a bending radius of 15 mm could be handled.

Beside the calibration of the presented sensors arrays the high frequency calibration device may be used to compare them with industrial hot-film sensors. Furthermore the insulation effect of the water cover will be investigated using this tool.

Acknowledgments The authors would like to thank all the project partners for the cooperative and effective work in the framework of the collaborative research center 880. One of the authors (S. B.) gratefully acknowledges the financial support of the Volkswagen Foundation. T. B. also thanks the colleagues at CMST from Ghent University and IMEC Ghent for the nice integration into their group and their cooperation.

References

Berns A, Buder U, Obermeier E, Wang XH, Domhardt J, Leuckert J, Nitsche W (2008) AeroMEMS pressure sensor with integrated wall hot-wire. IEEE Sens Conf 1560–1563. doi:10.1109/ICSENS.2008.4716746

Buder U, Berns A, von Klitzing J, Obermeier E, Petz R, Nitsche W (2006) Family of micromachined wall hot-wire sensors on polyimide foil. AIAA J (August 2007) 1798–1809. doi:10.2514/1.25033

Burkhardt O (2004) Erprobung und Anwendung von Oberflächensensoren und Sensorarrays zur Erfassung instationärer Wandschubspannungen an Schaufelprofilen. Dissertation, Technische Universtität Berlin, Berlin

Davis M (1970) The dynamic response of constant resistance anemometers. J Phys E Sci Instrum 3:15–20

De Vries JWC (1988) Temperature and thickness dependence of the resistivity of thin polycrystalline aluminum, cobalt, nickel, palladium, silver and gold films. Thin Solid Films, Electron Opt 25–32. doi:10.1016/0040-6090(88)90478-6

DuPont (2011) DuPont Kapton HN Technical Datasheet. http://www2.dupont.com/Kapton/en_US/assets/downloads/pdf/HN_datasheet.pdf. Accessed 29 July 2013

Ebefors T (2000) Polyimide V-groove joints for three-dimensional silicon transducers. Dissertation, Royal Institute of Technology, Stockholm. ISBN: 91-7170-568-6

Eckelmann H (1997) Einführung in die Strömungsmeßtechnik. Teubner Verlag, Stuttgart. ISBN: 3-519023792

Frühauf J (2005a) Shape and functional elements of the bulk silicon microtechnique. Springer, Heidelberg. ISBN: 3-540-22109-3

Frühauf J (2005b) Werkstoffe der Mikrotechnik. Fachbuchverlag Leipzig im Hanser Verlag, Leipzig. ISBN: 3-44622-557-9

Gad-El-Hak M (ed.) (2001) MEMS handbook. CRC Press LLC, Boca Raton, Florida, p 938ff. ISBN: 0-8493-0077-0

Haynes WM (2010) CRC handbook of chemistry and physics, 91st edn. Taylor & Francis group, Boca Raton. ISBN: 978-1-4398-2077-3

HD MicroSystems (2009) Product bulletin: PI 2600 series—low stress applications. http://hdmicrosystems.com/HDMicroSystems/en_US/pdf/PI-2600_ProcessGuide.pdf. Accessed 29 July 2013

Kälvesten E (1996) Pressure and wall shear stress sensors for turbulence measurements. Dissertation, Royal Institute of Technology, Stockholm. ISSN: 0281-2878

Kim IC, Lee SJ (2006) Characterization of a miniature thermal shear-stress sensor with backside connections. Sens Actuators 128:305–311

King LV (1914) On the convection of heat from small cylinders in a stream of fluid: determination of the convection constants of small platinum wires with applications to hot-wire anemometry. Philos Trans R Soc RSTA 214(509–522):373–432. doi:10.1098/rsta1914.0023

Lienhard IV JH, Lienhard V JH (2005) A heat transfer textbook. Phlogiston Press, Cambridge

Mailly F, Giani A, Bonnot R, Templ-Boyer P, Pascal-Delannoy F, Foucaran A, Boyer A (2001) Anemometer with hot platinum thin film. Sens Actuators 94, 1–2: 32–38

Morrison JF, Birch DM, Lavoie P (2006) IUTAM symposium on flow control and MEMS, vol 7. Springer, Heidelberg. ISBN: 978-1-4020-6857-7

Riedl X, Bolzmacher C, Wagner C, Bauer K (2009) A novel PDMS based capacitive pressure sensor. IEEE Sens Conf 2255–2258. doi:10.1109/ICSENS.2010.5690709

Rohlfing H, Schmidt H (1993) "Friedrich" Tabellenbuch Elektrotechnik Elektronik, 552 edn. Dümmler, Bonn. ISBN: 3-427-53024-8

Shackelford J, Alexander W (2001) Materials science and engineering handbook. CRC Press, Boca Raton. ISBN: 0-8493-2696-6